Osteoarthritis and Cartilage 18 (2010) 909–916

Osteoarthritis and Cartilage

In-vivo time-dependent articular cartilage contact behavior of the tibiofemoral joint

A. Hosseini †‡, S.K. Van de Velde †, M. Kozanek †, T.J. Gill †, A.J. Grodzinsky ‡§, H.E. Rubash †, G. Li †*

† *Bioengineering Laboratory, Department of Orthopaedic Surgery, Massachusetts General Hospital/Harvard Medical School, Boston, MA 02114, USA*
‡ *Department of Mechanical Engineering, Massachusetts Institute of Technology, Cambridge, MA 02139, USA*
§ *Department of Biological Engineering, Massachusetts Institute of Technology, Cambridge, MA 02139, USA*

ARTICLE INFO

Article history:
Received 27 January 2010
Accepted 21 April 2010

Keywords:
Cartilage
Articular cartilage
In-vivo cartilage contact behavior
Time-dependent
Cartilage contact deformation
Cartilage contact area

SUMMARY

Objective: The purpose of this study was to investigate the *in-vivo* time-dependent contact behavior of tibiofemoral cartilage of human subjects during the first 300 s after applying a constant full body weight loading and determine whether there are differences in cartilage contact responses between the medial and lateral compartments.
Design: Six healthy knees were investigated in this study. Each knee joint was subjected to full body weight loading and the *in-vivo* positions of the knee were captured by two orthogonal fluoroscopes during the first 300 s after applying the load. Three-dimensional models of the knee were created from MR images and used to reproduce the *in-vivo* knee positions recorded by the fluoroscopes. The time-dependent contact behavior of the cartilage was represented using the peak cartilage contact deformation and the cartilage contact area as functions of time under the constant full body weight.
Results: Both medial and lateral compartments showed a rapid increase in contact deformation and contact area during the first 20 s of loading. After 50 s of loading, the peak contact deformation values were $10.5 \pm 0.8\%$ (medial) and $12.6 \pm 3.4\%$ (lateral), and the contact areas were 223.9 ± 14.8 mm^2 (medial) and 123.0 ± 22.8 mm^2 (lateral). Thereafter, the peak cartilage contact deformation and contact area remained relatively constant. The respective changing rates of cartilage contact deformation were $1.4 \pm 0.9\%$/s (medial) and $3.1 \pm 2.5\%$/s (lateral); and of contact areas were 40.6 ± 20.8 mm^2/s (medial) and 24.0 ± 11.4 mm^2/s (lateral), at the first second of loading. Beyond 50 s, both changing rates approached zero.
Conclusions: The peak cartilage contact deformation increased rapidly within the first 20 s of loading and remained relatively constant after ~50 s of loading. The time-dependent response of cartilage contact behavior under constant full body weight loading was significantly different in the medial and lateral tibiofemoral compartments, with greater peak cartilage contact deformation on the lateral side and greater contact area on the medial side. These data can provide insight into normal *in-vivo* cartilage function and provide guidelines for the improvement of *ex-vivo* cartilage experiments and the validation of computational models that simulate human knee joint contact.

Introduction

Numerous studies have investigated articular cartilage contact in order to understand the intrinsic biomechanical characteristics of cartilage and its associated pathologies such as cartilage degeneration in medial and lateral compartments. Biomechanically, articular cartilage has been viewed as a biphasic material[1]. The *in-vitro* response of articular cartilage to various simulated loading conditions has been studied using pressure sensors[2–4], imaging techniques[5], and finite element methods[6]. For example, in most *in-vitro* studies that employed magnetic resonance imaging (MRI) to investigate the cartilage, the tibiofemoral joint was first loaded for a certain amount of time to deform as desired and then scanned[7]. Analogously, the biphasic nature of cartilage tissue under various loading conditions has been analyzed extensively using indentation and confined/unconfined compression tests[1,8–10]. However, due to the complexity of the *in-vivo* loading conditions, it is a challenge to simulate *in-vivo* physiological cartilage responses in an *in-vitro* experimental setup.

In-vivo studies have also described changes in the thickness and volume of the knee joint cartilage after dynamic activities such as bending, running, normal gait and squatting[11]. Although the studies based on this type of pre-loading protocol could provide long-term

* Address correspondence and reprint requests to: G. Li, Bioengineering Laboratory, MGH/Harvard Medical School, 55 Fruit Street, GRJ 1215, Boston, MA 02114, USA. Tel: 1-617-726-6472; Fax: 1-617-724-4392.
E-mail address: gli1@partners.org (G. Li).

1063-4584/$ – see front matter
doi:10.1016/j.joca.2010.04.011

cartilage contact data, the time-dependent response of tibiofemoral cartilage to an external load remains unclear, especially the *short-term* response of tibiofemoral cartilage. In addition, no data have been reported on the specific contact behavior of the medial and lateral compartments of the knee, even though varying degrees of osteoarthritis (OA) have been described in the knee hemi-joints[12]. These data would be critical for understanding the function of cartilage and investigating pathologies of the cartilage.

Recently, a combined Dual Fluoroscopic Imaging System (DFIS) and MRI technique has been used to study the *in-vivo* cartilage contact location[13]. Furthermore, the instantaneous tibiofemoral cartilage contact deformation during *in-vivo* physiological activities such as lunge and gait has been investigated using this technique[14–16]. The objective of this study was to investigate the time-dependent responses of the tibiofemoral cartilage under a constant body weight load and determine whether the medial and lateral compartments show differences in time-dependent contact behavior. The combined DFIS and MRI technique was employed to measure the real-time tibiofemoral cartilage contact deformation as well as the contact area, as the characteristics of the cartilage contact behavior, in the medial and lateral compartments of the knee joint.

Method

Subject selection

Six human knees, with no history of injury or proprioceptive defects upon physical and radiographic (MRI and X-ray) examination, were investigated in this study. All knees were from healthy males aged between 30 and 45 years and with average body mass index (BMI) of 24.8 kg/m^2. The study was approved by our institutional review board and written consent was obtained from all the participants. All the subjects were asked to refrain from any strenuous activities such as running, lifting, stair climbing for at least 4 h prior to their visit and to remain seated (non-weight-bearing position) for 2 h prior to the MRI scan of the knee to reduce the effect of residual cartilage deformation[14].

MRI and 3D model of knee

Each knee was scanned in sagittal, coronal and transverse planes using a 3 T MR scanner (MAGNETOM Trio®, Siemens, Malvern, PA, USA) with the subject supine and the knee in a relaxed, extended position. The MRI scanner was equipped with a surface coil and a 3D double echo water excitation sequence (field of view: 160 mm × 160 mm × 120 mm, image resolution: 512 × 512 pixels, voxel resolution: 0.31 mm × 0.31 mm × 1.00 mm, time of repetition: 24 ms, time of echo: 6.5 ms and flip angle: 25°)[14]. The MR images were imported into a solid modeling software package (Rhinoceros®, Robert McNeel & Associates, Seattle, WA, USA) to construct the 3D surface mesh models of the tibia, femur, fibula, and articulating cartilage using a protocol established in our laboratory[17]. The meshes were assembled using a point density of 80 vertices/cm^2 and triangular facets, with an average aspect ratio of 2. A typical 3D knee joint model is shown in Fig. 1(A).

Dual fluoroscopic imaging and reproduction of knee kinematics

A DFIS was used to capture the *in-vivo* kinematics of the knee joints. The DFIS was constructed using two fluoroscopes (BV Pulsera®, Philips, Bothell, WA, USA) with their intensifiers positioned in orthogonal planes providing a cubic imaging space of ~300 mm × 300 mm × 300 mm and image resolution of 1024 × 1024 pixels (0.29 mm × 0.29 mm). A force plate with a six degrees-of-freedom (6DOF) load cell (JR3®, Inc., Woodland, CA, USA) was incorporated into the DFIS to simultaneously record the ground reaction forces during loading [Fig. 1(B)]. The load cell had a resolution of 0.5 N with data acquisition rate of 1 kHz. Each knee joint was imaged for 300 s (timing and recording were started at the moment of foot-force plate contact) *while the subject stood still on the testing leg under full body weight*. Two supporting bars were incorporated into the DFIS to help stabilize the subject during the single-leg upright standing for 300 s. For the first 5 s, the knee was imaged at a rate of 15 frames per second. Then, the images were captured every 5 s up to 50 s, and finally every 20 s up to 300 s.

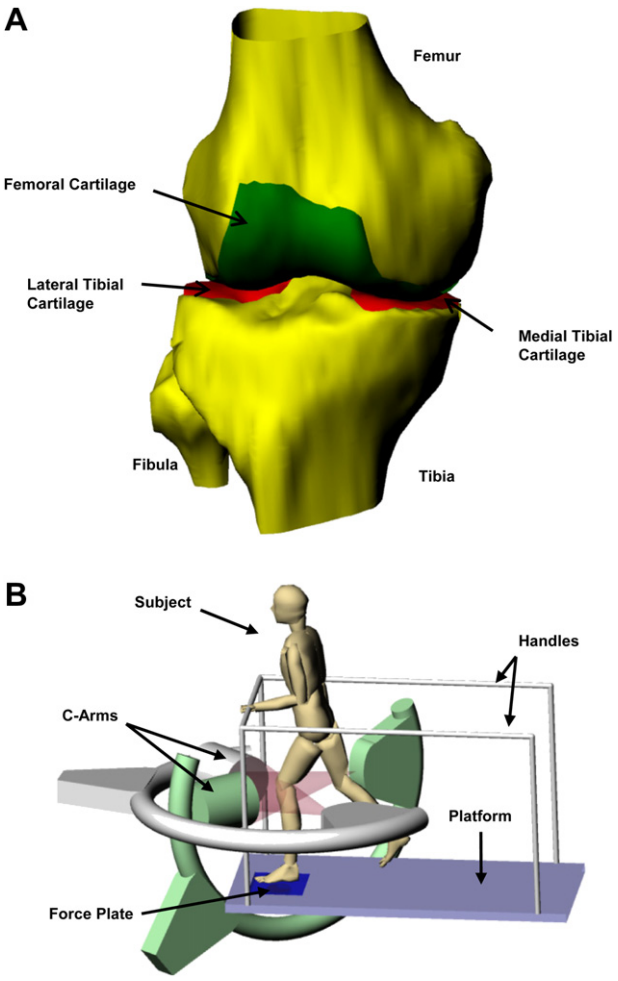

Fig. 1. (A) A three-dimensional (3D) knee model constructed using the series of MR images of a subject's knee. (B) Schematic of the DFIS.

The pairs of fluoroscopic images were imported into the solid modeling software and placed in orthogonal planes based on the geometry of the fluoroscopes (the relative positions of the intensifiers and the X-ray sources) during the experiment to create a 'virtual' DFIS[18]. The 3D MRI-based bony models of the knee joint were then imported into the virtual DFIS, viewed from two orthogonal directions corresponding to the setup of the fluoroscopes' X-ray sources (Fig. 2). The knee models were translated and rotated independently in 6DOF until the projection of the model matched the outlines of corresponding bones on the imported images obtained at each time point. When the projections matched with the pair of orthogonal images taken *in-vivo*, the models reproduced the *in-vivo* positions of the knee bones inside the software. The matching process was done manually in this study. The mesh models of the femoral and tibial cartilages (built from the

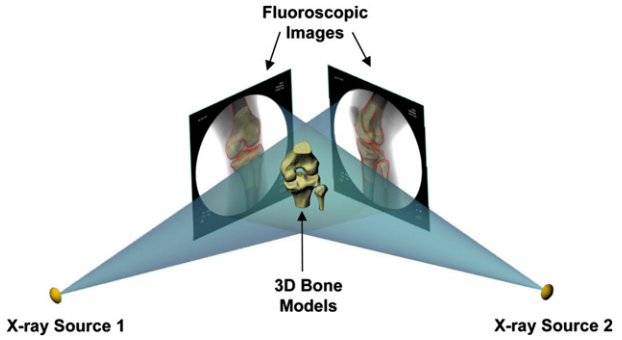

Fig. 2. Reproduction of kinematics of the tested knee joint in a virtual DFIS. Each bony model was individually matched with corresponding fluoroscopic images, viewed from two different directions.

relaxed position of the knee during MRI) were then imported and mapped onto the bony models at each time point. The accuracy of the system in reproducing knee kinematics using the above technique was reported <0.1 mm and $<0.3^\circ$ in translation and rotation respectively[19].

In-vivo cartilage contact behavior

At each reproduced *in-vivo* position of the knee joint, cartilage contact was defined as the overlap of the tibial and femoral cartilage surface meshes (Fig. 3). *Contact area* (mm^2) was defined as the area of a patch surface which was fitted to the curve made from the intersection of the overlapped cartilage meshes.

Cartilage contact deformation (%) was calculated at each vertex of the articular surface mesh as the amount of penetration (mm) divided by the sum of the tibial and femoral cartilage surface thicknesses (mm) at the same place, multiplied by 100[14,15]. Penetration was calculated as the minimum Euclidian distance connecting a vertex of the reference cartilage mesh to the opposite intersecting cartilage mesh. The peak contact deformation was determined as the maximum contact deformation at each time point. *The rate of change* of the cartilage contact deformation (%/s) was defined and calculated as the change in the cartilage contact deformation at two consecutive time points divided by the time interval over which it occurred. Similarly, the rate of change of contact area (mm^2/s) was calculated.

A previous validation study showed an accuracy of 4% when this technique was used to measure the cartilage contact deformation in human ankle joint[20]. Furthermore, the accuracy of cartilage thickness measurement using MRI-based model of the knee joint has been validated and reported to be 0.04 ± 0.01 mm [mean $\pm$ standard deviation (SD)][15].

Statistical analysis

To study the time-dependent contact behavior of tibiofemoral cartilage, the peak contact deformation at medial and lateral compartments was reported as a function of time. In addition, the cartilage contact area change with time was determined. A two-way repeated measures analysis of variance and a *post hoc* Student–Newman–Keuls test were used to determine the statistically significant differences in contact area and cartilage contact deformation between the medial and lateral compartments as a function of time (Statistica© StatSoft, Inc., Tulsa, OK, USA). Level of significance was set at <0.05.

Results

The peak cartilage contact deformation, as well as the cartilage contact area of both the medial and lateral compartments of the individual knee joints are presented in Tables I and II. The average peak cartilage contact deformation over time as well as the rate of change of the cartilage contact deformation (mean $\pm$ SD) are shown in Fig. 4 for the medial and lateral tibial compartments. Figure 5 presents the average cartilage contact area as well as its rate of change for both compartments. In all of the cases, the vertical component of the ground reaction force – measured with the load platform – reached the full body weight of the subject within approximately 1 s.

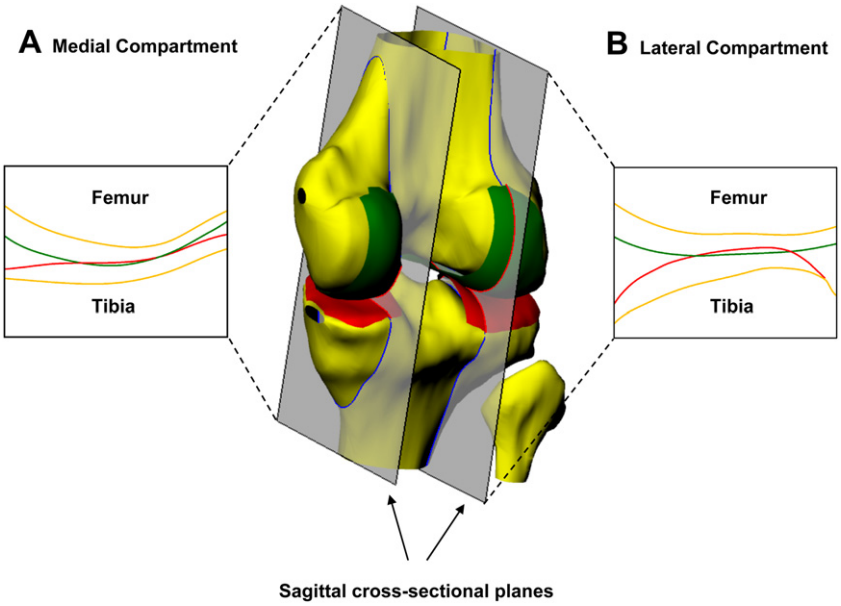

Fig. 3. Patterns of contact deformation in the tibiofemoral cartilage: (A) **Medial compartment**: contact is occurring on the concave (conforming) surface of medial tibial cartilage, (B) **Lateral compartment**: contact is occurring on the convex surface of lateral tibial cartilage.

Table I
Cartilage contact deformation (%) as a function of time under full body weight

Time (s)	Knee 1		Knee 2		Knee 3		Knee 4		Knee 5		Knee 6	
	Medial	Lateral	Medial	Lateral	Medial	Lateral	Medial	Lateral	Medial	Lateral	Medial	Lateral
0	5.0	5.8	1.7	0.7	4.9	1.9	4.6	1.6	3.4	5.3	4.6	0.1
5	8.6	10.0	5.1	9.0	8.2	5.6	8.9	5.2	8.8	11.0	7.4	11.3
10	8.9	13.4	6.0	8.8	8.7	6.3	9.1	5.4	9.2	12.4	7.9	13.0
15	9.1	14.7	8.9	9.8	9.3	6.7	9.3	5.4	9.7	13.3	8.2	13.0
20	9.5	14.9	8.8	10.6	9.2	7.2	9.9	5.8	9.8	14.5	8.8	14.1
25	10.0	15.3	9.2	11.6	9.4	7.3	9.7	6.1	9.7	15.0	8.4	13.7
30	10.8	15.9	9.5	12.0	10.2	7.6	10.2	6.9	10.5	15.6	8.7	13.5
50	11.5	16.4	10.7	12.4	10.7	9.4	10.5	7.9	10.8	15.0	8.9	14.7
70	11.4	16.5	11.7	13.1	11.5	9.9	11.2	9.0	11.5	14.8	9.8	15.0
90	11.2	16.5	12.7	15.4	11.8	10.1	10.8	8.6	11.5	15.2	10.5	13.9
110	10.9	16.6	12.1	16.0	12.7	9.9	11.2	8.8	12.0	15.6	9.3	14.3
150	10.9	17.4	12.4	15.7	12.8	9.8	10.4	7.9	11.5	14.7	10.8	14.3
190	11.2	17.5	13.2	17.1	12.1	10.2	11.1	8.3	11.9	14.7	10.2	15.0
210	11.2	17.3	11.8	17.5	12.3	10.3	10.9	8.1	11.5	15.4	10.4	16.0
250	11.9	17.4	11.9	18.6	12.6	10.9	11.5	8.5	13.0	14.6	11.2	16.3
290	12.2	17.8	12.8	18.5	13.2	10.9	11.6	8.7	12.3	15.3	9.9	15.9
300	12.6	18.4	13.4	18.2	13.1	10.8	11.5	8.9	12.5	15.6	9.5	16.0

Cartilage contact deformation and area with time

Medial compartment

The peak contact deformation was measured $4.0 \pm 1.3\%$ when the tested leg contacted with the ground (time zero). The corresponding cartilage contact area was $47.0 \pm 21.2\ mm^2$. At the first second of loading, the peak values of cartilage contact deformation and the cartilage contact area were $5.4 \pm 1.7\%$ and $87.6 \pm 33.1\ mm^2$. At this moment, the loading had reached 89.7% of full body weight. At 10 s of loading, the peak cartilage contact deformation sharply increased to $8.3 \pm 1.2\%$, representing a 105.4% increase in the magnitude compared to that at the beginning of the loading. The corresponding cartilage contact area was $174.2 \pm 19.7\ mm^2$. The peak contact deformation further increased to $10.5 \pm 0.8\%$, with a contact area of $223.9 \pm 14.8\ mm^2$ at 50 s of loading. Thereafter, the peak cartilage contact deformation was relatively constant and reached $12.1 \pm 1.4\%$ at 300 s of loading with a corresponding contact area of $263.2 \pm 19.6\ mm^2$. The contours of contact deformation distribution of a typical subject in the sagittal cross-section of medial compartment are shown in Fig. 6(A).

Lateral compartment

At time zero, the peak cartilage contact deformation was $2.6 \pm 2.4\%$ with a corresponding contact area of $20.3 \pm 20.3\ mm^2$. At 10 s of loading, the peak cartilage contact deformation was $9.9 \pm 3.2\%$, representing 19.2% more deformation in comparison with that measured in medial compartment. The contact area increased to $94.8 \pm 24.9\ mm^2$, representing a 45.6% decrease in contact area with respect to the medial compartment. After 50 s, the magnitude of the peak cartilage contact deformation reached $12.6 \pm 3.4\%$ and a contact area of $123.0 \pm 22.8\ mm^2$. Thereafter, both the peak contact deformation and contact area remained relatively constant and were $14.6 \pm 3.9\%$ and $135.6 \pm 20.8\ mm^2$ at 300 s, respectively. At this time point, the peak deformation in the lateral compartment was 21% greater than that in the medial compartment, whereas the contact area was 48.5% less than that in the medial side. The contours of contact deformation distribution of a typical subject in the sagittal cross-section of the lateral compartment are shown in Fig. 6(B).

Rate of change

Medial compartment

The deformation rate reached its peak of $1.4 \pm 0.9\%/s$ at the first second of loading. The rate of change of the contact area also experienced its peak value of $40.6 \pm 20.8\ mm^2/s$ at this time point. The rate of change in the peak deformation and contact area quickly decreased to $0.1 \pm 0.0\%/s$ and $4.2 \pm 1.3\ mm^2/s$, respectively at the

Table II
Contact area (mm^2) as a function of time under full body weight

Time (s)	Knee 1		Knee 2		Knee 3		Knee 4		Knee 5		Knee 6	
	Medial	Lateral	Medial	Lateral	Medial	Lateral	Medial	Lateral	Medial	Lateral	Medial	Lateral
0	37.5	24.3	12.0	5.0	52.8	20.0	76.1	21.1	50.0	31.2	53.8	20.0
5	155.1	85.9	103.7	99.8	149.3	50.0	172.4	69.3	162.9	100.0	176.2	110.8
10	167.4	99.0	147.1	105.8	161.8	59.0	179.0	70.8	187.3	109.6	202.8	124.6
15	174.9	106.9	175.4	110.8	173.4	63.6	187.4	72.6	197.1	120.5	213.4	127.2
20	175.5	110.8	181.6	118.0	190.9	66.9	196.2	77.2	200.4	127.4	224.5	135.4
25	187.8	120.4	202.4	123.9	195.8	69.2	194.5	81.8	200.0	134.4	225.9	142.2
30	192.2	120.0	204.8	126.8	200.0	74.0	207.2	89.7	207.4	135.8	231.0	140.6
50	207.1	127.1	212.9	130.0	231.1	91.0	218.2	99.7	225.5	144.5	248.4	145.5
70	211.5	128.0	213.0	131.3	240.0	95.4	230.9	107.4	241.6	144.3	255.3	148.6
90	212.4	125.5	228.9	136.6	262.0	97.9	237.8	106.7	245.4	152.8	259.1	150.4
110	208.8	123.5	232.1	142.3	277.8	97.7	246.1	110.6	252.9	154.6	257.2	153.0
150	213.2	126.8	238.2	150.7	273.1	100.0	248.7	106.2	262.0	152.0	252.2	154.6
190	233.1	128.2	230.0	142.2	269.5	100.5	265.5	106.7	263.1	151.8	260.0	150.7
210	234.7	122.5	237.3	142.5	270.9	100.3	265.5	106.2	264.6	157.1	256.0	152.9
250	238.7	124.5	230.4	145.2	284.0	103.1	267.2	106.4	267.9	154.6	261.6	155.6
290	231.5	131.2	230.9	149.1	291.0	106.4	272.3	113.3	266.2	156.7	262.9	151.7
300	241.1	133.1	242.7	147.5	292.6	106.9	273.9	115.5	268.4	156.0	260.4	154.7

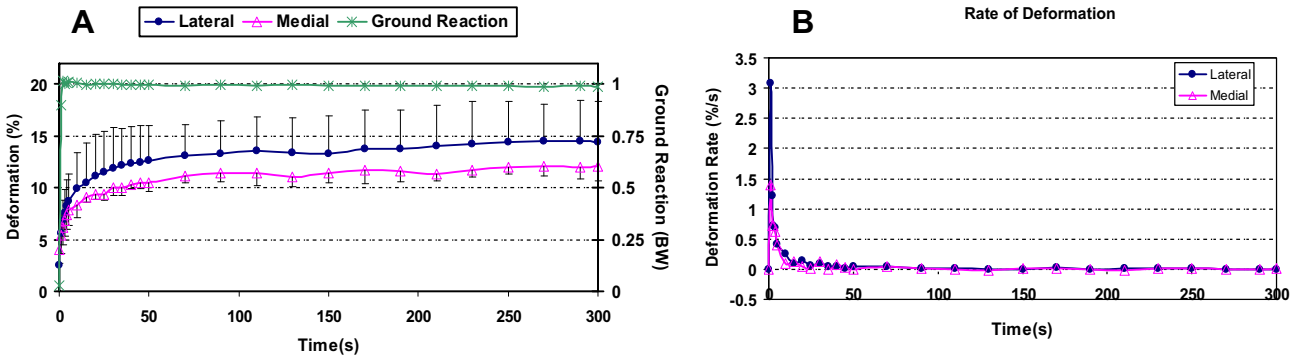

Fig. 4. (A) The variation of the peak cartilage contact deformation over time (mean ± SD) and the corresponding ground reaction force (normalized for body weight). (B) Mean values of the rate of change of the peak cartilage deformation in tibial compartments.

10th second of loading. Beyond about 50 s, no changes in rate of peak deformation and contact area were detectable within the measurement accuracy of our system.

Lateral compartment

Peak rate of change of the contact deformation and contact area (3.1 ± 2.5%/s and 24.0 ± 11.4 mm^2/s, respectively) was observed in first second of loading. These values represent that at the beginning of loading, the rate of change of the peak deformation curve was 2.2 times faster in the lateral compartment. However, the rate of change of the contact area was 1.7 times faster in the medial compartment. Thereafter, the rate of change of both deformation and contact area decreased quickly and after about 50 s of loading, no changes in the rate of peak deformation and contact area were detectable within the measurement accuracy our system.

Discussion

This study investigated the time-dependent contact of the articular cartilage of the human knee under constant full body weight loading during a single-leg standing using a combined dual fluoroscopic and MR imaging technique[18]. The peak cartilage contact deformation and the cartilage contact area as functions of time were determined. Both medial and lateral compartments of the tibial plateau were considered and compared to determine whether the hemi-joints show differences in contact behavior.

The cartilage contact deformation and contact area during the measured time interval (300 s) were found to sharply increase in the first 20 s even though the body weight reached constant within 1 s during the single-leg standing, and beyond 50 s, the cartilage contact deformation and contact area changed in a much lower rate. Generally, during the measured time interval, the lateral cartilage had greater peak contact deformation compared to medial side, while the cartilage contact area was greater in the medial compartment. The location of cartilage–cartilage contact indicated that the contact deformation occurred in the concave (conforming) surface in the medial compartment of tibia, while in the lateral compartment, the cartilage contact occurred at the convex surface of tibial cartilage (Fig. 3).

Previous studies have documented that tibial cartilage is thicker on the lateral plateau compared to that of the medial plateau[11,14]. The same pattern was observed in the current study (Table III). In reported *in-vivo* studies of the knee during lunge[14], the peak contact deformation of the medial compartment was reported to be greater than that in the lateral compartment (25 ± 9% and 22 ± 10%, respectively; at full extension). Also, during the stance phase of gait[16], the peak contact deformation of the medial compartment (ranging from 8 ± 5%, at the beginning of stance, to 23 ± 6%, at 30% of stance) was reported to be greater than that in the lateral compartment (ranging from 7 ± 3%, at the beginning of stance, to 16 ± 4%, at 30% of stance corresponding to full extension). Our data show that the *in-vivo* biomechanics of loading during single-leg standing is different. During the single-leg standing, the body is likely laterally inclined (body weight center shifts laterally) to keep stability, which may explain the higher contact deformation at the lateral compartment. Future studies should quantify the body weight center location with respect to the knee joint.

The peak deformation of knee cartilage (peak cartilage surface overlapping normalized by cartilage thickness) was less than the peak deformation that was measured in the ankle joint (32.3% at 300 s) during the single-leg standing[21]. Also, the rate of change of cartilage contact deformation was less than that previously measured in the ankle joint (1.4–3.1% vs 18.7%/s, respectively; at 1 s). However, it is interesting to note that the summation of medial

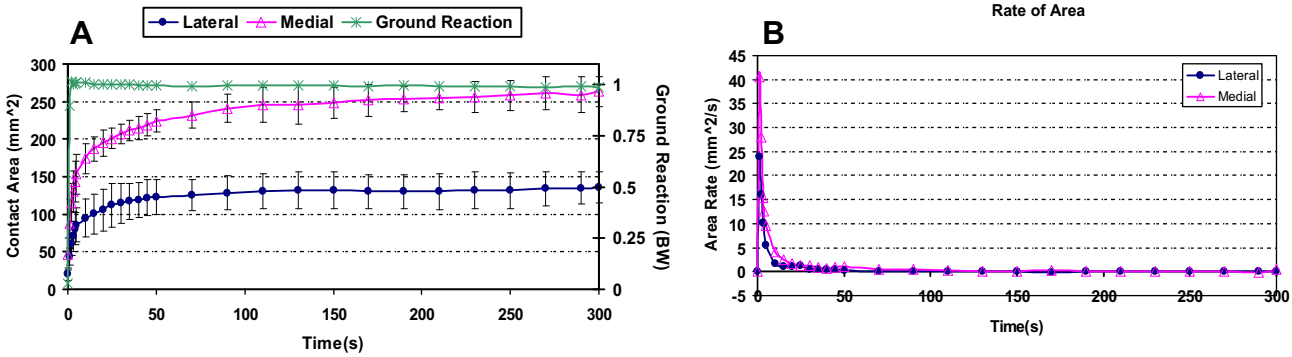

Fig. 5. (A) The variation of cartilage contact area over time (mean ± SD) and the corresponding ground reaction force (normalized for body weight). (B) Mean values of the rate of change of the cartilage contact area in tibial compartments.

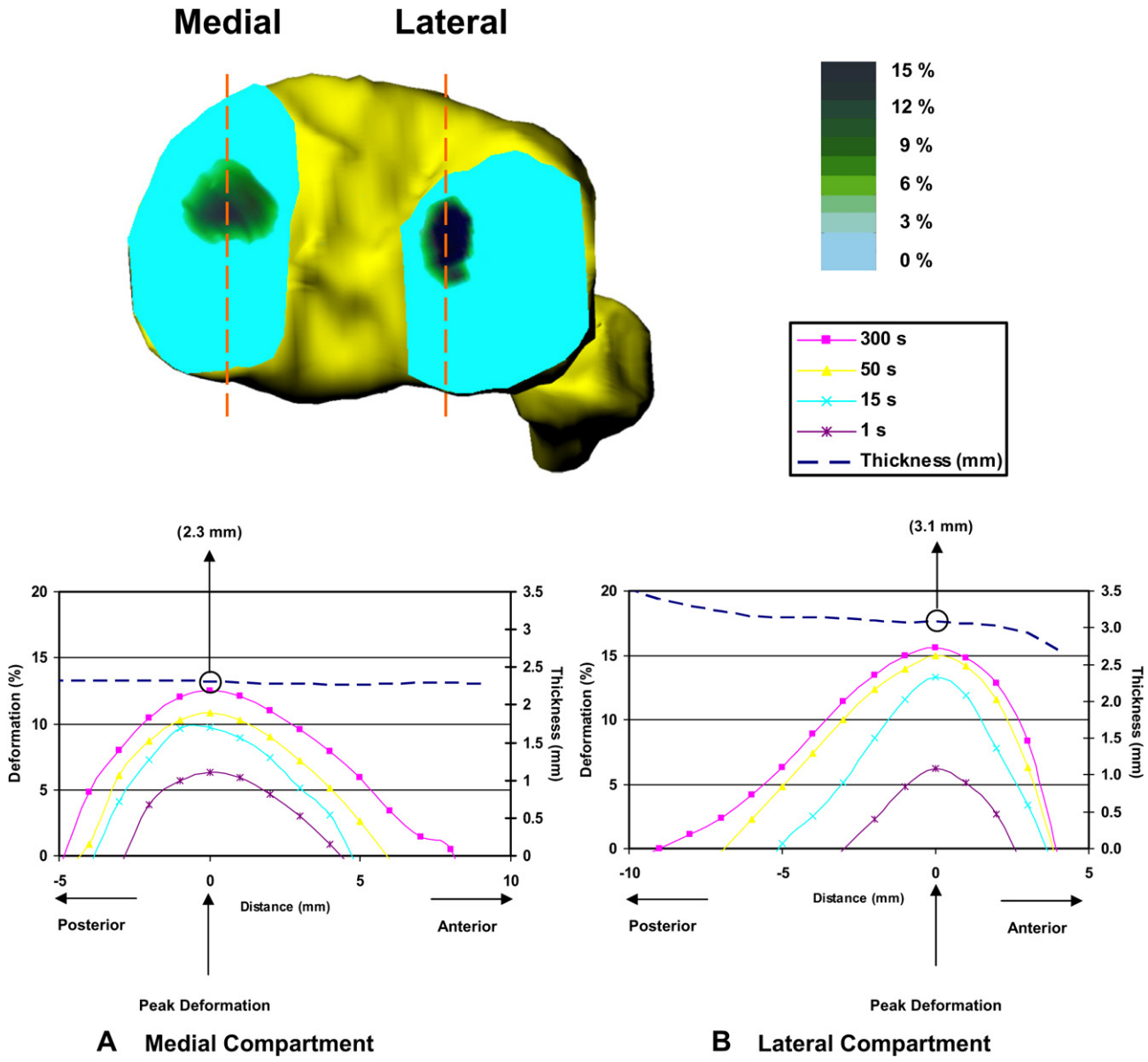

Fig. 6. Contours of contact deformation distribution of a typical subject in the course of time in the sagittal cross-sections (dashed lines) in medial and lateral compartments.

and lateral contact areas in articular cartilage of the knee was close to that of the human ankle. Ankle cartilage is much thinner than knee cartilage[20,22]. The average cartilage thickness was reported to be 1.4 ± 0.2 mm in the proximal talar cartilage[20], whereas in our study, it was 2.7 ± 0.5 mm and 3.2 ± 0.6 mm in the medial and lateral tibial compartments, respectively. Further, it is worth noting that in this study only cartilage–cartilage contact was investigated and meniscus–cartilage contact was not included. This might explain why the deformation in the knee joint was less than that of the ankle joint.

Table III
The thickness of tibial cartilage (mm) at the location of peak cartilage contact deformation

Knee	Thickness (mm)	
	Medial	Lateral
1	2.7	2.3
2	2.3	3.4
3	2.3	3.6
4	3.5	3.9
5	2.3	3.0
6	2.9	3.2
Mean ± SD	2.7 ± 0.5	3.2 ± 0.6

MR imaging techniques have been extensively used to study the effect of loading on the cartilage morphology[7,11]. However, due to the limitations such as long data acquisition time during MRI scanning and the time-dependent behavior of the cartilage itself, capturing the real-time deformation of the cartilage under a physiological loading presents a challenge. In most *ex-vivo* joint studies, the joint was first loaded for a certain amount of time to deform as desired and then scanned using MRI[7,23]. Thus, the MR imaging techniques might be adequate only for studying the long-term response of the cartilage to loadings[21]. Nevertheless, critical data have been reported on the volume and average thickness changes of the human knee cartilage after bending, squatting, running[11,24,25]. For example, Eckstein *et al.* have reported a $3.1 \pm 4.5\%$ and $2.4 \pm 5.2\%$ cartilage volume change in the medial and lateral tibial compartments, respectively, after 2 min of static

loading (squatting) on one leg at 15° of flexion with 200% body weight[11]. Additionally, Herberhold *et al.*, measured the cartilage deformation in a selected central 2D slice within the contact area and reported a 1.3% femoral cartilage deformation in the first minute of loading of 150% body weight (3% patellar cartilage deformation)[23]. Due to difference in the targeted joint, the measured deformation quantity (thickness, volume, etc.), as well as the type of loading and boundary conditions, it is difficult to compare those studies directly with the current study. In general, the cartilage deformations measured in the current study were relatively higher than those previously reported in the literature. Nevertheless, a significant difference in cartilage volumetric deformation between medial and lateral compartment has been similarly observed by Eckstein *et al.*[11]

While the determination of *in-vivo* cartilage contact deformation of the knee has been a challenge in biomechanical engineering, in *in-vitro* studies using bone–cartilage surfaces or cartilage explants, indentation tests and confined/unconfined compression tests have been widely employed to apply a constant force to investigate the creep behavior of the cartilage[1,26–30]. This phenomenon is similar to that observed in our data. Usually, a sharp increase in the deformation was observed in the initial seconds after applying the load, followed by a continuous creep for a long term. However, the physiological and biomechanical conditions in living tissue within intact joints differ substantially from those in experiments involving *post-mortem* specimens of cartilage or cartilage–bone plugs because of the influence of different boundary conditions and the fact that the integrity of the matrix has been changed at the edges of the tissue[25]. In reality, neither confined nor unconfined compression precisely mimics deformation of cartilage within intact (living) articular joints. Furthermore, in most *in-vitro* experiments (except during unconfined compression) the contact area is held constant. This type of experimental setup represents different biomechanical contact conditions compared to physiological conditions in which the contact area varies with time as shown in the present data (Fig. 5).

The data obtained in this study may have important implications in biomechanical studies of human cartilage. Different rates of OA in medial and lateral compartments have been reported in various studies[12]. By distinguishing the contact behavior of the two compartments during functional loading conditions, it may provide insights into the biomechanical factors that might be related to OA development. Clinically, numerous cartilage repair techniques have been proposed[31]. Our data might provide guidelines to evaluate the time-dependent behavior of the repaired cartilage. Further, in *ex-vivo* tests of time-dependent cartilage behavior, a selected load or deformation was applied to the specimen. Our data may provide useful information on the loading conditions to design *ex-vivo* experiments of cartilage specimens in order to simulate physiological responses of the cartilage. Finally, the *in-vivo* time-dependent contact responses of the cartilage can provide a physiological objective function to validate 3D finite element models that are established to simulate human knee joint functions.

Certain limitations of this study should be noted. Since the menisci deform and move in response to joint loading, and are invisible on current fluoroscopic images, the deformation of the menisci cannot be computed with the present methodology. Therefore, the meniscus–cartilage contact was not included in this study. Cartilage contact deformation was calculated based on the overlapping of the 3D models of tibial and femoral cartilages, and the deformation of the individual cartilage layers could not be determined. Using the overlap of the cartilage surface models to determine the cartilage contact area might overestimate the actual cartilage contact area, since the true cartilage is not penetrating through the contact, and therefore will deform and expand beyond the edge of the overlapping contact area. Another limitation was that the *in-vivo* forces in the medial and lateral compartments of the knee joint were not measured. Despite the above-mentioned limitations, the data on time-dependent contact behavior of human knee joint were determined under *in-vivo* physiological loading conditions.

In conclusion, this study investigated the *in-vivo* time-dependent contact behavior of human tibiofemoral articular cartilage under a constant full body weight. The cartilage deformation was found to sharply increase after loading. The contact area was greater in the medial than in the lateral compartment, while the peak contact deformation was greater in the lateral compartment. These data could provide insight into normal *in-vivo* cartilage function, and may be instrumental for the design of relevant *ex-vivo* experiments that are aimed to investigate, for instance, the chondrocyte mechanotransduction under physiological loading conditions. Further, *in-vivo* cartilage contact data are necessary for validation of 3D computational models which are used to predict the intrinsic biomechanical responses of the articular joints.

Author contributions

All authors were involved in drafting the article or revising it critically for important intellectual content, and all authors approved the final version to be published. Dr. Li had full access to all of the data in the study and takes responsibility for experimental design, the integrity of the data, and the accuracy of the data analysis.

Study conception and design: Hosseini, Van de Velde, Kozanek, Gill, Grodzinsky, Rubash, Li.

Provision of study materials or patients: Hosseini, Van de Velde, Kozanek, Gill, Grodzinsky, Rubash, Li.

Acquisition of data: Hosseini, Van de Velde, Kozanek, Li.

Analysis and interpretation of data: Hosseini, Van de Velde, Kozanek, Gill, Grodzinsky, Rubash, Li.

Conflict of interest

The authors have declared no conflicts of interest.

Acknowledgements

The authors gratefully acknowledge the financial support of the National Institute of Health (R01 AR055612, F32 AR056451) and the Department of Orthopaedic Surgery at the Massachusetts General Hospital. We would also want to thank the volunteers who participated in this study and Bijoy Thomas for his technical assistance.

Role of the funding source: the authors gratefully acknowledge the financial support of the National Institute of Health (R01 AR055612, F32 AR056451) and the Department of Orthopaedic Surgery at the Massachusetts General Hospital. The funding sources had no involvement in the study design; in the collection, analysis, and interpretation of data; in the writing of the report; and in the decision to submit the paper for publication.

References

1. Mow VC, Kuei SC, Lai WM, Armstrong CG. Biphasic creep and stress relaxation of articular cartilage in compression? Theory and experiments. J Biomech Eng 1980;102:73–84.
2. Guettler JH, Demetropoulos CK, Yang KH, Jurist KA. Dynamic evaluation of contact pressure and the effects of graft harvest with subsequent lateral release at osteochondral donor sites in the knee. Arthroscopy 2005;21:715–20.

3. D'Agata SD, Pearsall AW, Reider B, Draganich LF. An in vitro analysis of patellofemoral contact areas and pressures following procurement of the central one-third patellar tendon. Am J Sports Med 1993;21:212–9.
4. Hsieh YF, Draganich LF, Ho SH, Reider B. The effects of removal and reconstruction of the anterior cruciate ligament on the contact characteristics of the patellofemoral joint. Am J Sports Med 2002;30:121–7.
5. Neu CP, Hull ML, Walton JH, Buonocore MH. MRI-based technique for determining nonuniform deformations throughout the volume of articular cartilage explants. Magn Reson Med 2005;53:321–8.
6. Haut Donahue TL, Hull ML, Rashid MM, Jacobs CR. The sensitivity of tibiofemoral contact pressure to the size and shape of the lateral and medial menisci. J Orthop Res 2004;22:807–14.
7. Naish JH, Xanthopoulos E, Hutchinson CE, Waterton JC, Taylor CJ. MR measurement of articular cartilage thickness distribution in the hip. Osteoarthritis Cartilage 2006;14:967–73.
8. Ateshian GA, Warden WH, Kim JJ, Grelsamer RP, Mow VC. Finite deformation biphasic material properties of bovine articular cartilage from confined compression experiments. J Biomech 1997;30:1157–64.
9. Lee RC, Frank EH, Grodzinsky AJ, Roylance DK. Oscillatory compressional behavior of articular cartilage and its associated electromechanical properties. J Biomech Eng 1981;103:280–92.
10. Treppo S, Koepp H, Quan EC, Cole AA, Kuettner KE, Grodzinsky AJ. Comparison of biomechanical and biochemical properties of cartilage from human knee and ankle pairs. J Orthop Res 2000;18:739–48.
11. Eckstein F, Lemberger B, Gratzke C, Hudelmaier M, Glaser C, Englmeier KH, *et al*. In vivo cartilage deformation after different types of activity and its dependence on physical training status. Ann Rheum Dis 2005;64:291–5.
12. Felson DT, Nevitt MC, Zhang Y, Aliabadi P, Baumer B, Gale D, *et al*. High prevalence of lateral knee osteoarthritis in Beijing Chinese compared with Framingham Caucasian subjects. Arthritis Rheum 2002;46:1217–22.
13. Li G, Park SE, DeFrate LE, Schutzer ME, Ji L, Gill TJ, *et al*. The cartilage thickness distribution in the tibiofemoral joint and its correlation with cartilage-to-cartilage contact. Clin Biomech (Bristol, Avon) 2005;20:736–44.
14. Bingham JT, Papannagari R, Van de Velde SK, Gross C, Gill TJ, Felson DT, *et al*. In vivo cartilage contact deformation in the healthy human tibiofemoral joint. Rheumatology (Oxford) 2008;47:1622–7.
15. Van de Velde SK, Bingham JT, Hosseini A, Kozanek M, Defrate LE, Gill TJ, *et al*. Increased tibiofemoral cartilage contact deformation in patients with anterior cruciate ligament deficiency. Arthritis Rheum 2009;60:3693–702.
16. Liu F, Kozanek M, Hosseini A, Van de Velde SK, Gill TJ, Rubash HE, *et al*. In vivo tibiofemoral cartilage deformation during the stance phase of gait. J Biomech 2009.
17. Li G, DeFrate LE, Park SE, Gill TJ, Rubash HE. In vivo articular cartilage contact kinematics of the knee: an investigation using dual-orthogonal fluoroscopy and magnetic resonance image-based computer models. Am J Sports Med 2005;33:102–7.
18. Li G, Wuerz TH, DeFrate LE. Feasibility of using orthogonal fluoroscopic images to measure in vivo joint kinematics. J Biomech Eng 2004;126:314–8.
19. Li G, Van de Velde SK, Bingham JT. Validation of a non-invasive fluoroscopic imaging technique for the measurement of dynamic knee joint motion. J Biomech 2008;41:1616–22.
20. Wan L, de Asla RJ, Rubash HE, Li G. In vivo cartilage contact deformation of human ankle joints under full body weight. J Orthop Res 2008;26:1081–9.
21. Li G, Wan L, Kozanek M. Determination of real-time in-vivo cartilage contact deformation in the ankle joint. J Biomech 2008;41:128–36.
22. Athanasiou KA, Niederauer GG, Schenck Jr RC. Biomechanical topography of human ankle cartilage. Ann Biomed Eng 1995;23:697–704.
23. Herberhold C, Faber S, Stammberger T, Steinlechner M, Putz R, Englmeier KH, *et al*. In situ measurement of articular cartilage deformation in intact femoropatellar joints under static loading. J Biomech 1999;32:1287–95.
24. Eckstein F, Tieschky M, Faber SC, Haubner M, Kolem H, Englmeier KH, *et al*. Effect of physical exercise on cartilage volume and thickness in vivo: MR imaging study. Radiology 1998;207:243–8.
25. Eckstein F, Tieschky M, Faber S, Englmeier KH, Reiser M. Functional analysis of articular cartilage deformation, recovery, and fluid flow following dynamic exercise in vivo. Anat Embryol (Berl) 1999;200:419–24.
26. Frank EH, Grodzinsky AJ. Cartilage electromechanics—I. Electrokinetic transduction and the effects of electrolyte pH and ionic strength. J Biomech 1987;20:615–27.
27. Frank EH, Grodzinsky AJ. Cartilage electromechanics—II. A continuum model of cartilage electrokinetics and correlation with experiments. J Biomech 1987;20:629–39.
28. Mow VC, Gibbs MC, Lai WM, Zhu WB, Athanasiou KA. Biphasic indentation of articular cartilage—II. A numerical algorithm and an experimental study. J Biomech 1989;22:853–61.
29. Armstrong CG, Lai WM, Mow VC. An analysis of the unconfined compression of articular cartilage. J Biomech Eng 1984;106:165–73.
30. Boschetti F, Pennati G, Gervaso F, Peretti GM, Dubini G. Biomechanical properties of human articular cartilage under compressive loads. Biorheology 2004;41:159–66.
31. Bedi A, Feeley BT, Williams RJ. 3rd Management of articular cartilage defects of the knee. J Bone Joint Surg Am 2010;92:994–1009.